



Synergistic effects in atomic-layer-deposited PtCox/CNTs catalysts enhancing hydrolytic dehydrogenation of ammonia borane



Jiankang Zhang^{a,b}, Wenyao Chen^c, Huibin Ge^{a,b}, Chaoqiu Chen^{a,*}, Wenjun Yan^a, Zhe Gao^a, Jie Gan^c, Baiyan Zhang^{a,b}, Xuezhi Duan^{c,*}, Yong Qin^{a,*}

^a State Key Laboratory of Coal Conversion, Institute of Coal Chemistry, Chinese Academy of Sciences, Taiyuan 030001, PR China

^b University of Chinese Academy of Sciences, Beijing 100039, PR China

^c State Key Laboratory of Chemical Engineering, East China University of Science and Technology, Shanghai, 200237, PR China

ARTICLE INFO

Keywords:

Atomic layer deposition
Pt-Co synergy
Ammonia borane
Hydrogen evolution
Kinetic and isotopic analyses

ABSTRACT

Highly dispersed and narrowly size-distributed Pt-Co bimetallic nanoparticles supported on CNTs are fabricated by atomic layer deposition (ALD) of Pt followed by CoO ALD for hydrolytic dehydrogenation of ammonia borane. The controlled decoration of CoO significantly enhances the hydrogen evolution activity of the Pt-based catalysts due to the remarkable Pt-Co synergy, i.e., the TOF value is up to $675.1 \text{ mol}_{\text{H}_2} \text{ mol}_{\text{Pt}}^{-1} \text{ min}^{-1}$ for bimetallic PtCo20/CNTs catalyst, which is 1.8 times higher than that of monometallic Pt/CNTs catalyst. The underlying nature of the Pt-Co synergy is systematically investigated by combining multiple characterizations with kinetic and isotopic analyses. It is revealed that the decoration of CoO onto Pt provides unique Pt-Co interfaces and targeted Pt electronic properties, thereby exhibiting the lower activation energy and favorable O–H bond cleavage being the rate-determining step for the hydrolysis reaction. The insights revealed here provide inspiration and guide for the rational design of other advanced nanocatalysts.

1. Introduction

Hydrogen (H_2) has been regarded as an alternative and promising energy carrier to address energy and environmental crisis. While how to securely store and efficiently release of H_2 are the two major barriers for the wide application of hydrogen energy [1–5]. Catalytic dehydrogenation of ammonia borane (AB) through hydrolysis has attracted increasing attention for H_2 production owing to the high hydrogen content of AB (19.6 wt%) and mild reaction conditions [6–13]. Pt-based catalysts, one of the most investigated catalysts both in scientific and industrial fields, exhibit much higher hydrogen evolution rates than other metal catalysts for hydrolysis of AB [14–18]. Coupling Pt with non-noble metals such as cobalt is an effective and practical method to enhance its catalytic performance by bimetallic synergy. Although many bimetallic catalysts have been developed for various reactions including AB hydrolysis [19–23], insightful understanding of nature of the bimetallic synergy is still a challenging issue due to the difficulty in precisely tuning catalyst's structure by traditional methods.

Atomic layer deposition (ALD) is an alternative catalyst synthesis method with precise tuning of catalyst's structure and particle size. ALD has been widely applied to synthesize catalysts with unique structure and excellent activity in recent years [16,24–30], and it is especially

attractive for the preparation of bimetallic catalysts with finely controllable structure [31–35]. The outstanding advantages of ALD endow it a powerful approach to quantitatively investigate structure–property relationship.

In this work, we synthesized a series of PtCox/CNTs (x represents CoO ALD cycle numbers) catalysts with finely controllable Pt–CoO interfaces by ALD to clarify the underlying nature of Pt–Co synergy for AB dehydrogenation reaction and study the dehydrogenation mechanism. The deposition of CoO significantly enhances the hydrogen evolution activity of the Pt-based catalysts due to the remarkable Pt–Co synergy. Multiple structure and electronic characterizations, as well as kinetic and isotopic analyses, were conducted to illuminate the structure–property relationship of PtCox/CNTs catalysts and dehydrogenation mechanism.

2. Experimental

2.1. Catalyst preparation

Raw CNTs (Surface area: $40\text{--}70 \text{ m}^2 \text{ g}^{-1}$, diameter: 40–60 nm), purchased from Shenzhen Nanotech Port Co. Ltd, were refluxed in HNO_3 (68 wt%) at 120°C for 6 h to remove the residual metals and amorphous

* Corresponding authors.

E-mail addresses: chenchaqiu@sxicc.ac.cn (C. Chen), xzduan@ecust.edu.cn (X. Duan), qinyong@sxicc.ac.cn (Y. Qin).

carbon, and then washed with deionized water to pH = 7, followed by drying at 90 °C for 10 h. Monometallic Pt/CNTs catalysts were prepared by ALD in a homemade closed chamber-type ALD reactor with (methylcyclopentadienyl)trimethylplatinum (MeCpPtMe₃) and ozone as Pt precursor and reactant gas, respectively. And the detailed information can be found in our previous reports.^{27, 34} For bimetallic PtCox/CNTs catalysts, the second metal (CoO) was deposited onto Pt/CNTs with bis (cyclopentadienyl) cobalt (Cp₂Co) as the cobalt precursor. MeCpPtMe₃ and Cp₂Co contained in stainless steel bubbler were heated to 60 °C and 66 °C respectively to provide enough vapor pressure. For all the catalysts, the deposition temperature was maintained at 280 °C, and the Pt ALD cycle number was 20. The amount of CoO was controlled by controlling the number of CoO ALD cycle. The as-prepared catalysts were denoted as PtCox/CNTs (x = 0, 5, 20, 40 and 100 ALD cycles).

2.2. Catalyst characterizations

The crystal structure and composition of the samples were examined by XRD (Bruker D8 Advance, Cu K α radiation ($\lambda = 1.540 \text{ \AA}$)). The morphology and microstructure of the catalysts was characterized by TEM and HRTEM (JEOL-2100F). Temperature programmed reduction (TPR) and Pt dispersion measurements were conducted in an Auto-Chem 2920 instrument. The X-ray photoelectron spectra (XPS) measurements were carried out with an ESCALab-250 X-ray photoelectron spectrometer (Al K α , 1486.6 eV). The X-ray absorption spectroscopy experiments were conducted on the BL14W1 beamline of the Shanghai Synchrotron Radiation Facility. The metal loading of the catalysts was measured by ICP-MS analysis (Thermo ICAP 6300).

2.3. Catalytic dehydrogenation tests

The hydrogenation evolution activity of the samples for AB hydrolytic dehydrogenation was tested at 25 \pm 0.5 °C. Briefly, the catalysts were firstly dispersed in deionized water (10 mL) placed in a round-bottom flask, and then 48 mg of AB (Aldrich, 97%) was added under stirring (700 rpm). The amount of hydrogen evolved during the reaction was measured in a typical water-filled gas burette by monitoring the displacement of water level every 0.25 min.

3. Results

3.1. Catalyst characterizations

The PtCox/CNTs catalysts with highly dispersed nanoparticles were synthesized by sequentially depositing Pt and CoO nanoparticles on CNTs via Pt and CoO ALD, respectively. As shown in Fig. 1, the quite weak peak at around 39.7° is observed in all the samples, which can be readily indexed as (111) crystal plane of face-centered cubic Pt° (JCPDS No.65–2868) [17,18], suggesting the small size and/or high dispersion

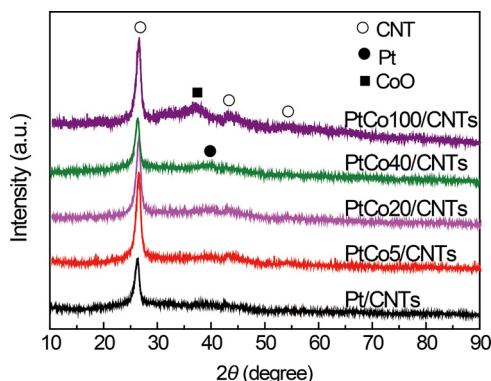


Fig. 1. XRD patterns of the PtCox/CNTs catalysts.

of the ALD-prepared Pt nanoparticles. The peak related to CoO is detected only in PtCo100/CNTs catalyst with relatively higher cobalt content, which further verifies the advantages of ALD in synthesizing small nanoparticles with high dispersion.

To further examine the morphology and microstructure of Pt/CNTs and representative PtCo20/CNTs catalysts, TEM and HRTEM were conducted. As shown in Fig. 2a-d, highly dispersed Pt and Pt-Co nanoparticles are uniformly deposited onto CNTs. Both of the catalysts present narrow particle size distributions, as shown in the insets in Fig. 2a and c. The average nanoparticle size of PtCo20/CNTs catalyst is about 2.4 nm, which is only a little larger than that of Pt/CNTs catalyst (1.8 nm), which is due to the deposition of CoO on/next to Pt forming Pt-Co interfaces (Fig. 2d). Fig. 2b and d show the typical HRTEM images of Pt/CNTs and PtCo20/CNTs catalysts, respectively. The measured distance between adjacent lattice fringes of the Pt nanoparticle is 0.223 nm (Fig. 2b), which corresponds well with the lattice spacing of the (111) planes of face-centered cubic Pt (fcc-Pt). For the bimetallic PtCo20/CNTs catalyst, besides (111) and (200) planes of fcc-Pt, (111) plane of CoO corresponding lattice spacing of 0.245 nm are also detected in the nanoparticle (inset in yellow frame, Fig. 2d), proving the co-existence of Pt and CoO in the nanoparticles. The sample was also characterized by HAADF-STEM and energy-dispersive X-ray spectroscopy mapping (Fig. 2e), which again confirm the high dispersion of ALD-synthesized Pt-Co bimetallic nanoparticles and uniform distribution of Pt and Co elements on CNTs.

Fig. 3a presents the normalized Pt L₃-edge X-ray absorption near-edge structure (XANES) spectra of Pt/CNTs and PtCo20/CNTs. The white line intensity of the two samples fall in range between the white line of reference Pt foil and PtO₂, indicating that Pt nanoparticles contain a certain amount of platinum oxides besides metallic Pt°. Fig. 3b shows the Fourier transform of Pt L₃-edge extended X-ray absorption fine structure (EXAFS) oscillations for the corresponding samples. For PtCo20/CNTs sample, R space EXAFS spectra in Pt L₃ edge shows a slight shift in radial distribution compared to that of Pt/CNTs, which further indicates the interaction of Pt and Co [36,37]. These results indicate that CoO is deposited on or next to Pt nanoparticles and correspondingly modifies the electronic properties of Pt and constructs targeted Pt-Co interfaces.

From the X-ray photoelectron spectra (XPS) survey and Co2p spectra of the catalysts (Fig. S1a-b), C, O, Pt and Co peaks are observed, confirming again the successful deposition of Pt and CoO onto CNTs. The introduction of CoO species has a direct influence on Pt4f binding energy and subtle difference can be found (Fig. 4a and Table S1), i.e., an appreciable shift to higher values of Pt4f_{7/2} binding energy is observed in the PtCox/CNTs bimetallic catalysts compared to that of monometallic Pt/CNTs, implying that there exists electron transfer from Pt to CoO in these bimetallic catalysts. Thus the as-prepared bimetallic catalysts contain positively charged Pt, and the extent of electron-deficiency increases with an increased Co content (i.e., CoO ALD cycle numbers). In addition, the intensity of Pt4f decreases gradually with increasing numbers of CoO ALD cycle from 0, 5 to 20 cycles, i.e., the ratio of peak intensity of Pt4f for these samples is about 1:0.82:0.57. However, no observable decrease is observed with the further increase of CoO ALD cycle numbers (Fig. 4b), which suggests that Pt is partially decorated/covered by CoO species even under higher Co content (40 or 100 cycle-CoO), i.e., Pt-Co interfaces are kept constant and CoO begins to grow on CNTs forming isolated larger CoO nanoparticles when the CoO ALD cycle number amounts to certain value (larger than 20), which is consistent with the above TEM and EXAFS results. This can be further demonstrated by H₂-temperature programmed reduction (H₂-TPR) characterization. As shown in Fig. 4c, a H₂ reduction peak attributed to the reduction of CoO at around 327 °C can be observed in the monometallic Co20/CNTs catalyst. However, the H₂ reduction peak shifts to much lower temperatures for the bimetallic PtCox/CNTs catalysts (no peaks were detected for the PtCo5/CNTs catalysts due to the low amount of CoO beyond detection limits of detector), demonstrating

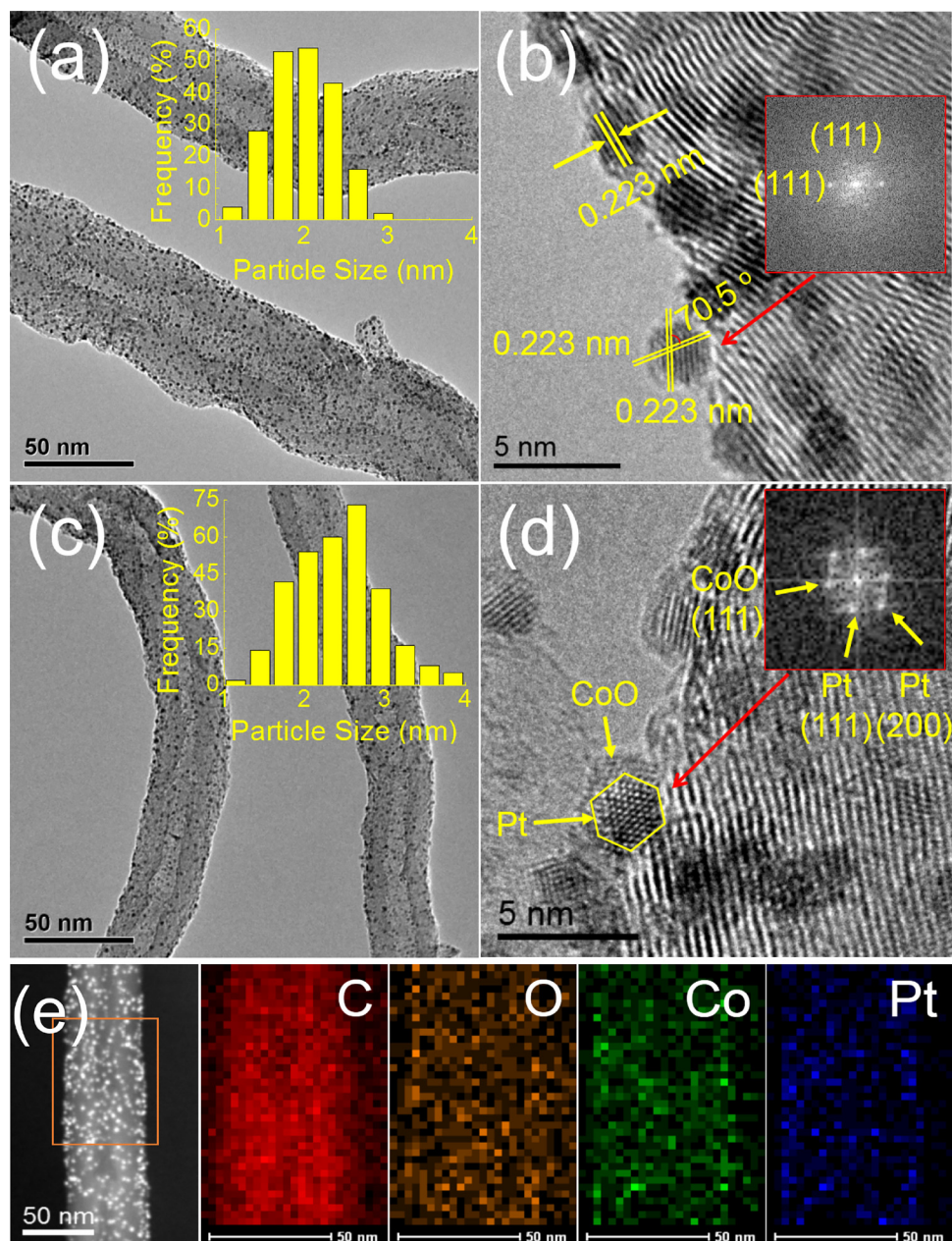


Fig. 2. TEM (a) and HRTEM (b) images of the as-synthesized Pt/CNTs and PtCo20/CNTs (c and d) catalysts. Elemental mappings of the rectangle area in (e) show the distribution of carbon, oxygen, cobalt and platinum, respectively. (Insets in (a) and (c): the corresponding histograms of particle size distribution, respectively; insets in (b) and (d): fast fourier transform of Pt and Pt-Co nanoparticles, respectively).

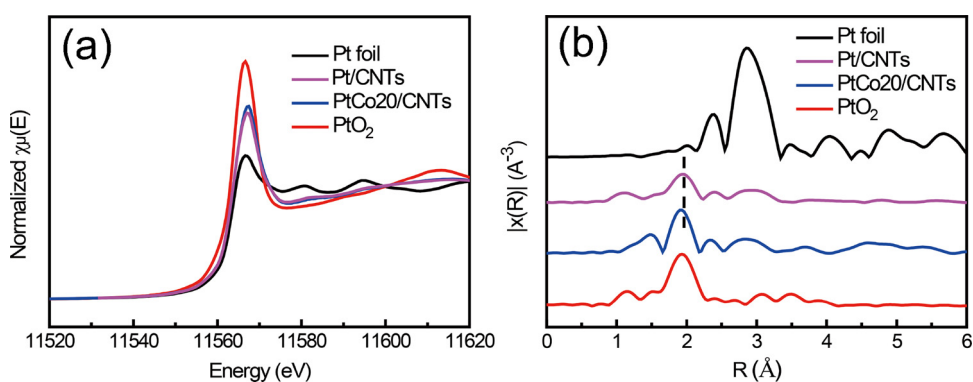


Fig. 3. (a) Pt L₃-edge XANES spectra for Pt foil, Pt/CNTs, PtCo20/CNTs and PtO₂. (b) The corresponding Fourier transform k^3 -weighted EXAFS spectra of the samples.

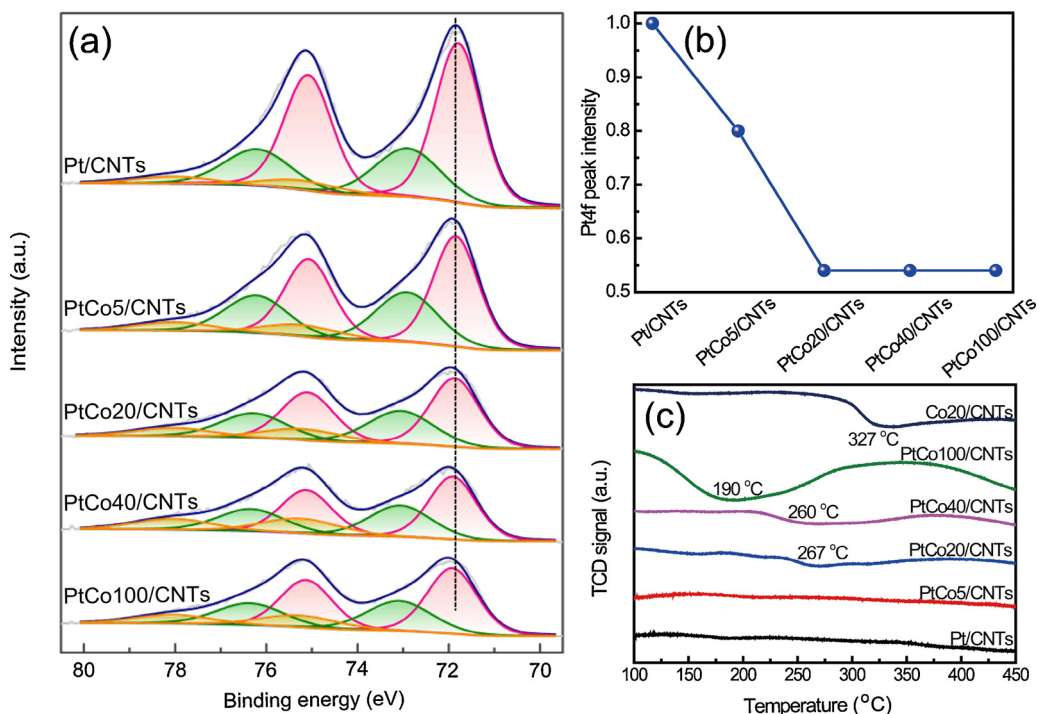


Fig. 4. (a) XPS Pt4f analysis of the as-prepared PtCox/CNTs catalysts and (b) the corresponding changes of Pt4f peak intensity. (c) H₂-TPR profiles of the as-prepared PtCox/CNTs and Co20/CNTs catalysts.

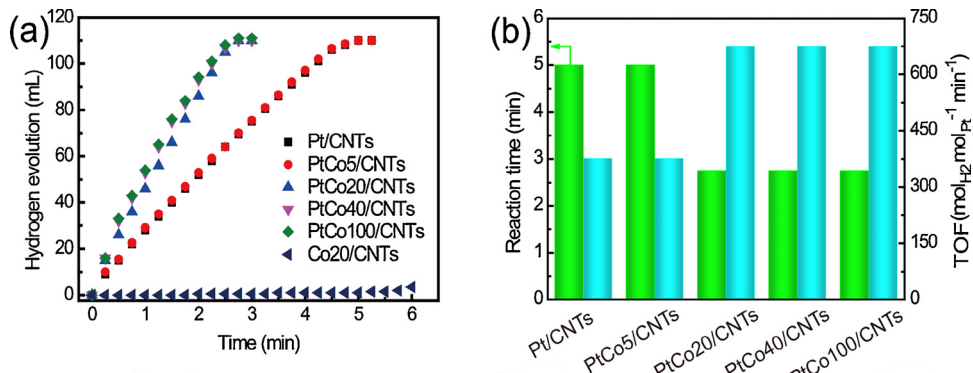
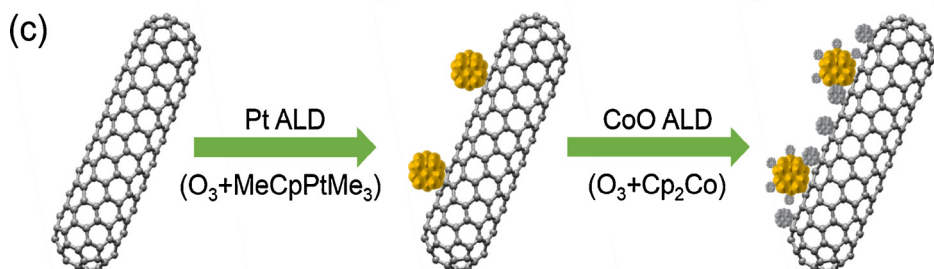


Fig. 5. (a) Volume of hydrogen evolved versus reaction time for AB dehydrogenation reaction (0.15 mol/L AB) at 25 ± 0.5 °C catalyzed by PtCox/CNTs and Co20/CNTs catalysts. (b) Time needed to complete the reaction and TOF values (obtained based on the overall Pt moles) of the PtCox/CNTs catalysts. (c) Schematic illustration of preparation of the PtCox/CNTs catalysts (x represents ALD cycle numbers of CoO).



that Pt has a strong promotion effect on the reduction of CoO due to hydrogen spillover effect [38–40]. And the reduction temperatures needed decrease monotonously by increasing numbers of CoO ALD cycle. This is because that CoO tends to grow on CNTs forming isolated larger CoO nanoparticles when the CoO ALD cycle numbers is higher than 20, and the larger CoO nanoparticles have weak interaction with CNT supports thus presenting lower reduction temperatures [41].

3.2. Catalytic dehydrogenation activity

The as-prepared monometallic Pt/CNTs and bimetallic PtCox/CNTs

catalysts were tested for the hydrolytic dehydrogenation of AB. Fig. 5a presents the volume of H₂ evolved versus reaction time over the PtCox/CNTs catalysts. For all the catalysts, a rapid and nearly linear hydrogen evolution curves was obtained without observable induction period. As expected, the relative Co content increases with the increase of CoO ALD cycle numbers (Table S1), and hydrogen evolution rate increases correspondingly (Fig. 5a,b). In other words, less reaction time is needed to complete the hydrolysis reaction, as shown in Fig. 5b. For example, when the CoO ALD cycle number increases to 20, corresponding to Co loading of 1.76 wt%, the needed reaction time decreases to 2.75 min, which is much shorter than that of monometallic Pt/CNTs catalyst

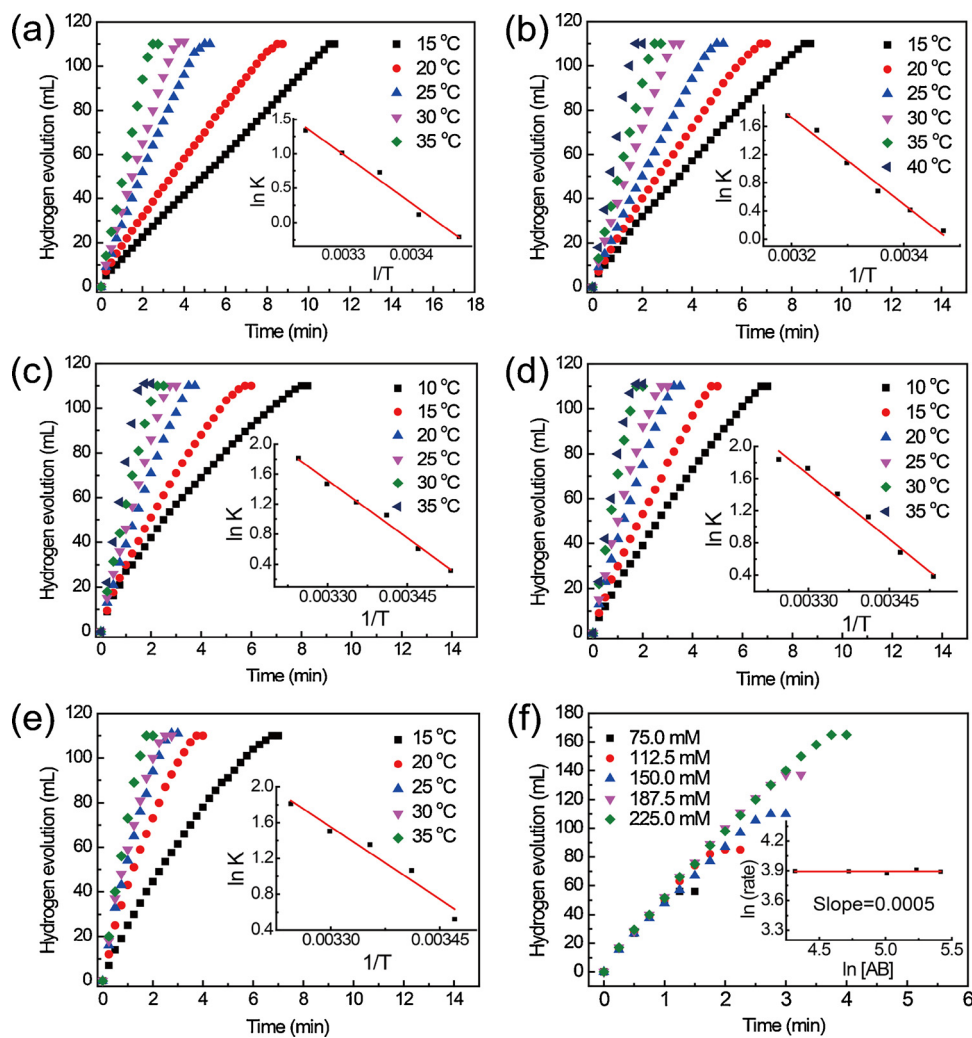


Fig. 6. Volume of hydrogen evolved versus reaction time for AB dehydrogenation reaction (0.15 mol/L AB) catalyzed by the as-prepared (a) Pt/CNTs, (b) PtCo5/CNTs, (c) PtCo20/CNTs, (d) PtCo40/CNTs and (e) PtCo100/CNTs catalysts at different temperatures. Insets in a-e: the corresponding Arrhenius plots of $\ln k$ vs. $1/T$. (f) Volume of hydrogen evolved versus reaction time for AB dehydrogenation reaction catalyzed by PtCo20/CNTs with different AB concentrations at $25 \pm 0.5^\circ\text{C}$.

(5 min). With the further increase of CoO ALD cycle numbers (40 and 100 cycles), no observable decrease is observed in view of the reaction time. These results indicate that appropriate amount of CoO addition (e.g., 20-cycle CoO) could significantly enhance the hydrogen evolution activity of the Pt/CNTs catalyst, i.e., the TOF values increase from 375.8 to 675.1 $\text{mol}_{\text{H}_2}\text{mol}_{\text{Pt}}^{-1} \text{min}^{-1}$ after decoration of 20-cycle CoO, which is higher than those of Pt-based catalysts reported previously. With the further increase of Co content (40 and 100-cycle CoO), only limited increase is observed in view of the initial hydrogen evolution rates (r_{initial} , see Fig. S2), suggesting that later deposited CoO is much less active than initially deposited CoO or further addition cobalt content has little effect on the enhancement of hydrogen evolution activity. This is probably because that the deposition position of CoO was changed with the increase of CoO ALD cycle numbers, i.e., the initially deposited CoO is decorated on the Pt nanoparticles forming CoO clusters and correspondingly fabricating Pt-Co unique interfaces, which have been demonstrated to be more catalytically active sites. With further increasing CoO ALD cycle number (40 and 100), the CoO tends to deposit both on initially CoO clusters and CNT supports nucleating and growing into larger CoO nanoparticles (Fig. 5c). In addition, the used catalysts can be magnetically separated after reaction by an external magnet due to the in situ reduction of cobalt oxide to metallic Co⁰ by spillover hydrogen generated in dehydrogenation reaction (Figs. S3 and S4). For comparison, the as-prepared Co20/CNTs catalyst with the

average particle size of 1.7 nm (Fig. S5) were also tested for AB dehydrogenation reaction, and only small amount of H_2 (about 3 mL) was released in the initial 6 min, indicating that Co20/CNTs catalyst is inactive for the reaction. These results indicate the remarkable promotional effect of cobalt species on the Pt-catalyzed hydrolytic dehydrogenation of AB, in which a suitable amount of the cobalt species can enhance the catalytic performance of Pt/CNTs significantly. In addition, the recyclability tests for the Pt/CNTs and representative PtCo20/CNTs catalysts were also carried out (Fig. S6). No obvious improvement was observed in view of the durability of the PtCo20/CNTs compared with Pt/CNTs, which may be ascribed to the agglomerations of metal nanoparticles and the adsorption of B-containing species on metal nanoparticles.¹⁷

3.3. Kinetic and isotopic analyses

In order to gain in-depth understanding of the Pt-Co synergy for AB dehydrogenation reaction, kinetic experiments of the five catalysts at 15–40 °C were conducted, as shown in Fig. 6a–e. For all the PtCo_x/CNTs catalysts, the dehydrogenation reaction is a zero-order reaction with respect to AB (also see Fig. 6f) [27,42], and thus the initial reaction rates can be described as $r = kc^n = k$ ($n = 0$), where k and c are the reaction rate constant and concentration of AB, respectively. k can be also correlated with activation energy (E_a) by the Arrhenius equation.

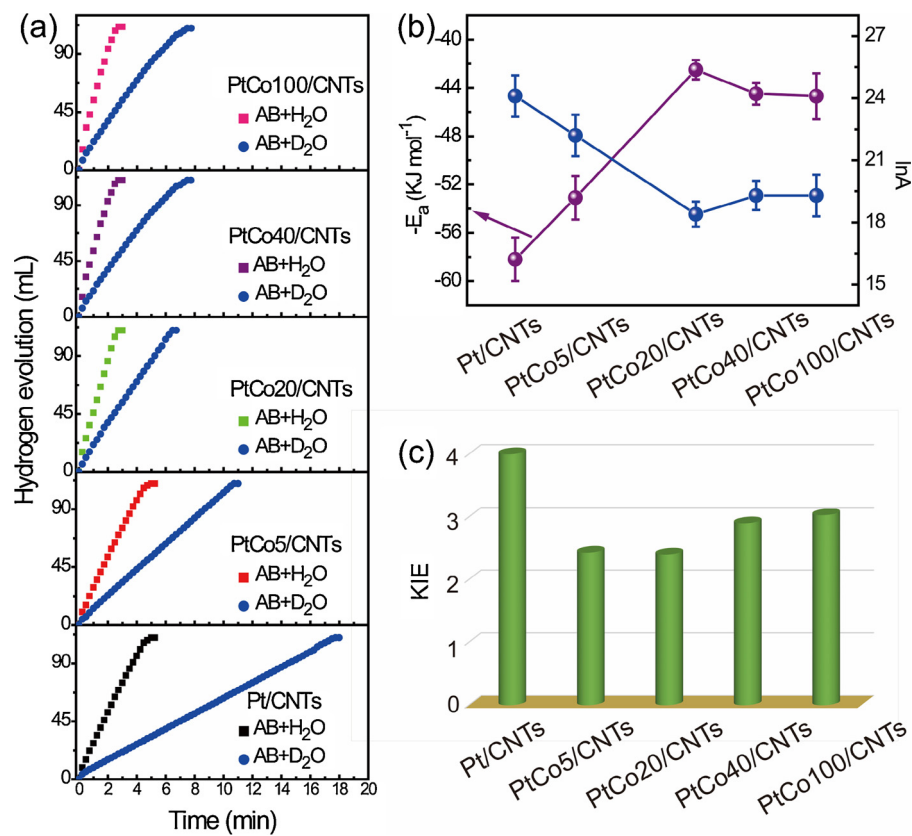


Fig. 7. (a) Volume of hydrogen evolved versus reaction time for AB dehydrogenation reaction (0.15 mol/L AB) at 25 \pm 0.5 °C catalyzed by PtCo_x/CNTs catalysts using H₂O and D₂O as the reactants. (b) E_a and lnA, and (c) KIE values of PtCo_x/CNTs catalysts.

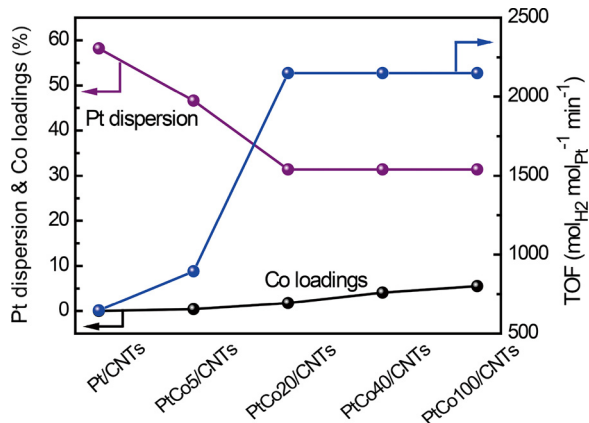


Fig. 8. TOF values with respect to Pt dispersion and Co loadings of the catalysts.

Hydrogen evolution rate constant k at these temperatures was calculated from the fitted linear portions of the plots to determine E_a . According to the Arrhenius plots of $\ln k$ versus $1/T$ (insets in Fig. 6a–e), E_a of the five catalysts were calculated to be about 58.2, 53.1, 42.5, 44.5 and 44.7 kJ mol⁻¹, respectively (Fig. 7b). As expected, the addition of CoO can decrease the E_a of the reaction and correspondingly accelerate hydrogen evolution rates. In addition, isotopic experiments using D₂O instead of H₂O were also carried out to gain mechanistic insights into the Pt-Co synergy and dehydrogenation mechanism. The kinetic isotope effect (KIE) values can be calculated by the ratio of rate constants with H₂O and D₂O as reactant respectively (i.e., $KIE = k_H/k_D$), which is regarded as a quite sensitive and essential means to determine whether the cleavage of O–H bond is the rate determining step for a given reaction [43,44]. Compared with H₂O as the reactant, all the catalysts, as

expected, present much slower hydrogen evolution rates using D₂O as the reactant (Fig. 7a). The KIE values of the five catalysts were calculated to be 4.00, 2.43, 2.40, 2.91 and 3.01, respectively (Fig. 7c), suggesting that the activation H₂O molecule or O–H bond cleavage should be occurred/involved in the rate determining step. It should be noted that all the bimetallic PtCo_x/CNTs catalysts exhibit much lower KIE values compared with monometallic Pt/CNTs catalyst, which indicates that the Pt–Co synergy in these bimetallic catalysts could promote the activation of H₂O molecule. Especially, the PtCo20/CNTs catalyst exhibits the lowest KIE value, demonstrating the strongest ability to active H₂O molecule of the catalysts. These results strongly demonstrate that deposition of CoO species on Pt/CNTs could contribute to the activation of H₂O molecule, lower the reaction E_a and correspondingly boost reaction activity.

4. Discussions

4.1. The role of Pt and CoO

Generally, noble metals (such as Pt, Rh, Ru etc.) are much more active than non-noble metals (such as Ni, Co, Cu etc.) for hydrolysis of AB [13–23]. While non-noble metal oxides are generally inactive for the hydrolysis of AB, as verified by our above mentioned Co20/CNTs catalyst, which is almost inactive for the hydrogen evolution in the initial period, i.e., only about 3 mL of H₂ was evolved in the initial 6 min (Fig. 5a,b). On the other hand, equivalent amount of H₂ (~108 mL) was completely released within 5 min on Pt/CNTs catalyst, which strongly indicates Pt is more efficient than CoO in view of the monometallic catalysts for the hydrolysis of AB. However, when the small amount of CoO (e.g., 20-cycle CoO) was added to Pt/CNTs synthesizing bimetallic PtCo20/CNTs catalyst, the hydrogen evolution rate increased greatly, i.e. the PtCo20/CNTs catalyst exhibits much higher hydrogen evolution

activity than the corresponding monometallic PtCo20/CNTs catalyst and physically mixed Pt/CNTs + Co20/CNTs catalysts without any Pt coverage (Figs. 5a,b and S7), which indicates that a remarkable synergy should be existed in the bimetallic PtCox/CNTs catalysts.

4.2. The Pt-Co synergy

According to the previous reports, hydrolytic dehydrogenation of AB is a surface sensitive reaction[13–17]. This can be also verified by our present study, i.e., the hydrogen evolution activity drops sharply when the Pt/CNTs is covered by only five ALD cycles of inactive ZnO (Fig. S8). On the contrary, the hydrogen evolution activity increase remarkably when the Pt/CNTs is decorated with a certain amount of CoO. To be noted that Pt metal surface is also covered by CoO in this case, as verified by the above XPS characterization. These results strongly demonstrate the existence of remarkable Pt-Co synergy in the PtCox/CNTs catalysts. To further elucidate this synergy, TOF values of the catalysts with respect to Pt dispersion (i.e., exposure fraction) as a function of Co content were constructed. The Pt dispersion of the monometallic Pt/CNTs was determined by pulse CO chemisorption method to be around 58.2% (Fig. S9), which is in accord with the TEM result (61.8%, according to the classic equation $D(\text{dispersion}) = 1.13/d$ (diameter, unit: nm) for hemispherical particles) [45]. For the bimetallic PtCox/CNTs catalysts, however, CO chemisorption were less reliable to determine the Pt dispersion because of interference by Co, i.e. the amount of adsorbed CO presents an increased tendency although the exposed Pt metal surface decreases (Fig. S9). And this can be ascribed to the interface synergistic catalysis effects, as reported by Somorjai's group [46]. Thus, the Pt dispersion of PtCox/CNTs catalysts were estimated semi-quantitatively according to their surface atomic ratios by XPS analyses (Table S1) using the Pt dispersion value of Pt/CNTs as reference (determined by CO chemisorption technology). Fig. 8 shows the plots of TOF values with respect to Pt dispersion and Co content (depended on the CoO ALD cycle numbers) of the catalysts. With the increase of Co content, the Pt dispersion or Pt fraction exposed of the PtCox/CNTs catalysts initially decreases greatly, reaches a minimum value when decorated by 20 cycle-CoO, and then remains stable with further increasing CoO amounts. Interestingly, the TOF values initially increase steeply, reach a maximum value when decorated by 20 cycle-CoO, and then remain stable. Especially, PtCo5/CNTs catalyst presents higher activity per Pt active site than that of Pt/CNTs catalyst in this regard, although the apparently activities of them are nearly identical (Fig. 5a). Combining these analyses and the above structure and electronic characterizations, as well as kinetic and isotopic results, we speculate that the boosting activities of PtCox/CNTs catalysts could be ascribed to the formation of unique Pt-Co interfaces and Pt-Co interaction through the interfaces (such as electron transfer from Pt to CoO). The PtCo20/CNTs catalyst reveals the best catalytic performance because the Pt-Co interfaces reach a maximum value when decorated by 20 cycle-CoO, and then remain stable with further increasing CoO ALD numbers.

5. Conclusions

Summarily, we have successfully synthesized a series of highly efficient PtCox/CNTs catalysts by ALD for hydrolysis of AB. The as-prepared PtCox/CNTs catalysts exhibit much higher hydrogen evolution rate than the monometallic Pt/CNTs catalyst due to Pt-Co synergy. The underlying nature of this synergy as well as catalyst's structure is verified by combining multiple characterizations, kinetic and isotopic analyses. The decoration of CoO on Pt provides unique Pt-Co interfaces and targeted Pt electronic properties, lowering the reaction E_a and promoting the cleavage of O–H bond being the rate-determining step for the hydrolysis reaction. The insights revealed here provide inspiration and guide for the rational design of other advanced bimetallic nanocatalysts.

Acknowledgements

We acknowledge the financial support from the National Natural Science Foundation of China (21203229 and 21673269), Natural Science Foundation of ShanXi Province (201701D121036) and Youth Innovation Promotion Association of the Chinese Academy of Sciences (2015139). We are grateful to Shanghai Institute of Applied Physics for the X-ray absorption spectroscopy measurement.

Appendix A. Supplementary data

Supplementary material related to this article can be found, in the online version, at doi:<https://doi.org/10.1016/j.apcatb.2018.04.070>.

References

- [1] Q. Zhu, Q. Xu, Phys. Energy Environ. Sci. 8 (2015) 478–512.
- [2] U.B. Demirci, P. Miele, Phys. Chem. Chem. Phys. 16 (2014) 6872–6885.
- [3] S. Akbayrak, Y. Tonbul, S. Özkar, Appl. Catal., B 198 (2016) 162–170.
- [4] J. Manna, S. Akbayrak, S. Özkar, Appl. Catal., B 208 (2017) 104–115.
- [5] C. Du, Q. Ao, N. Cao, L. Yang, W. Luo, G. Cheng, Int. J. Hydrogen Energy 40 (2015) 6180–6187.
- [6] W.-W. Zhan, Q.-L. Zhu, Q. Xu, ACS Catal. 6 (2016) 6892–6905.
- [7] Ö. Metin, V. Mazumder, S. Özkar, S. Sun, J. Am. Chem. Soc. 132 (2010) 1468–1469.
- [8] D. Sun, V. Mazumder, Ö. Metin, S. Sun, ACS Nano 5 (2011) 6458–6464.
- [9] H. Ma, C. Na, ACS Catal. 5 (2015) 1726–1735.
- [10] Q. Yao, W. Shi, G. Feng, Z.-H. Lu, X. Zhang, D. Tao, D. Kong, X. Chen, J. Power Sources 257 (2014) 293–299.
- [11] S. Akbayrak, M. Kaya, M. Volkan, S. Özkar, Appl. Catal., B 147 (2014) 387–393.
- [12] C.Y. Peng, L. Kang, S. Cao, Y. Chen, Z.S. Lin, W.F. Fu, Angew. Chem. Int. Ed. 54 (2015) 15725–15729.
- [13] L. Wang, H. Li, W. Zhang, X. Zhao, J. Qiu, A. Li, X. Zheng, Z. Hu, R. Si, J. Zeng, Angew. Chem. Int. Ed. 56 (2017) 4712–4718.
- [14] Q. Xu, M. Chandra, J. Alloy. Compd. 446 (2007) 729–732.
- [15] A. Ajaz, A. Karkamkar, Y.J. Choi, N. Tsumori, E. Rönnebro, T. Autrey, H. Shioyama, Q. Xu, J. Am. Chem. Soc. 134 (2012) 13926–13929.
- [16] M.A. Khalily, H. Eren, S. Akbayrak, H.H. Susapto, N. Biyikli, S. Özkar, M.O. Guler, Angew. Chem. Int. Ed. 128 (2016) 12445–12449.
- [17] W. Chen, D. Li, C. Peng, G. Qian, X. Duan, D. Chen, X. Zhou, J. Catal. 356 (2017) 186–196.
- [18] X. Wang, D. Liu, S. Song, H. Zhang, Chem. Commun. 48 (2012) 10207–10209.
- [19] D. Cléménçon, J. Petit, U. Demirci, Q. Xu, P. Miele, J. Power Sources 260 (2014) 77–81.
- [20] X. Yang, F. Cheng, J. Liang, Z. Tao, J. Chen, Int. J. Hydrogen Energy 36 (2011) 1984–1990.
- [21] H. Wang, L. Zhou, M. Han, Z. Tao, F. Cheng, J. Chen, J. Alloy Compd. 651 (2015) 382–388.
- [22] K. Mori, K. Miyawaki, H. Yamashita, ACS Catal. 6 (2016) 3128–3135.
- [23] Z. Li, T. He, D. Matsumura, S. Miao, A. Wu, L. Liu, G. Wu, P. Chen, ACS Catal. 7 (2017) 6762–6769.
- [24] H. Ge, B. Zhang, X. Gu, H. Liang, H. Yang, Z. Gao, J. Wang, Y. Qin, Angew. Chem. Int. Ed. 128 (2016) 7197–7201.
- [25] Z. Gao, M. Dong, G. Wang, P. Sheng, Z. Wu, H. Yang, B. Zhang, G. Wang, J. Wang, Y. Qin, Angew. Chem. Int. Ed. 54 (2015) 9006–9010.
- [26] C. Chen, P. Li, G. Wang, Y. Yu, F. Duan, C. Chen, W. Song, Y. Qin, M. Knez, Angew. Chem. Int. Ed. 52 (2013) 9196–9200.
- [27] J. Zhang, C. Chen, S. Chen, Q. Hu, Z. Gao, Y. Li, Y. Qin, Catal. Sci. Technol. 7 (2017) 322–329.
- [28] Z. Shang, S. Li, L. Li, G. Liu, X. Liang, Appl. Catal., B 201 (2017) 302–309.
- [29] J. Liu, J.W. Elam, P.C. Stair, Acc. Chem. Res. 46 (2013) 1806–1815.
- [30] J.A. Singh, N. Yang, S.F. Bent, Annu. Rev. Chem. Biomol. Eng. 8 (2017) 41–62.
- [31] E. Saarinen, M.C. Figueiredo, R. Karinen, A. Santasalo-Aarnio, H. Jiang, J. Sainio, T. Kallio, J. Lehtonen, Appl. Catal., B 148 (2014) 11–21.
- [32] N. Caner, A. Bulut, M. Yurderi, I.E. Ertas, H. Kivrak, M. Kaya, M. Zahmakiran, Appl. Catal., B 210 (2017) 470–483.
- [33] Y. Lei, B. Liu, J. Lu, R.J. Lobo-Lapidus, T. Wu, H. Feng, X. Xia, A.U. Mane, J.A. Libera, J.P. Greeley, Chem. Mater. 24 (2012) 3525–3533.
- [34] J. Zhang, Z. Yu, Z. Gao, H. Ge, S. Zhao, C. Chen, S. Chen, X. Tong, M. Wang, Z. Zheng, Y. Qin, Angew. Chem. Int. Ed. 56 (2017) 816–820.
- [35] Y. Shao, Z. Guo, H. Li, Y. Yu, X. Wang, Angew. Chem. Int. Ed. 56 (2017) 3226–3231.
- [36] K. Feng, J. Zhong, B. Zhao, H. Zhang, L. Xu, X. Sun, S.T. Lee, Angew. Chem. Int. Ed. 55 (2016) 11950–11954.
- [37] X. Wang, N. Li, C. Liu, L.D. Pfefferle, G.L. Haller, J. Mater. Chem. 22 (2012) 25083–25092.
- [38] L. He, Y. Huang, A. Wang, Y. Liu, X. Liu, X. Chen, J.J. Delgado, X. Wang, T. Zhang, J. Catal. 298 (2013) 1–9.
- [39] S.K. Beaumont, S. Alayoglu, C. Specht, W.D. Michalak, V.V. Pushkarev, J. Guo, N. Kruse, G.A. Somorjai, J. Am. Chem. Soc. 136 (2014) 9898–9901.
- [40] D. Nabaho, J.H. Niemantsverdriet, M. Claeys, E. van Steen, Catal. Today 261 (2016) 17–27.
- [41] J. Wang, H. Tan, S. Yu, K. Zhou, ACS Catal. 5 (2015) 2873–2881.

[42] M. Rakap, *Appl. Catal., B* 163 (2015) 129–134.

[43] Z. Li, T. He, L. Liu, W. Chen, M. Zhang, G. Wu, P. Chen, *Chem. Sci.* 8 (2017) 781–788.

[44] K. Koh, M. Jeon, D.M. Chevrier, P. Zhang, C.W. Yoon, T. Asefa, *Appl. Catal. B* 203 (2017) 820–828.

[45] Licheng Bai, Xin Wang, Qiang Chen, Yifan Ye, Haoquan Zheng, Jinghua Guo, Yadong Yin, Chuabo Gao, *Angew. Chem. Int. Ed.* 55 (2016) 15656–15661.

[46] K. An, S. Alayoglu, N. Musselwhite, S. Plamthottam, Gr.m. Melaet, A.E. Lindeman, G.A. Somorjai, *J. Am. Chem. Soc.* 135 (2013) 16689–16696.